Journal of Non-Crystalline Solids 674 (2026) 123912

Contents lists available at ScienceDirect

Journal of Non-Crystalline Solids

journal homepage: www.elsevier.com/locate/jnoncrysol

Incorporation mechanisms of niobium into lithium borate glasses: Insights from solid state nuclear magnetic resonance and Raman spectroscopy

Rafaella Bartz Pena [a,b,*], Henrik Bradtmüller [a,b], Laureano Ensuncho [a,b], Marcos De Oliveira Jr. [a,b], Hellmut Eckert [a,b]

[a] São Carlos Institute of Physics, University of São Paulo, IFSC – USP,13566-590, São Carlos, SP, Brazil
[b] Center for Research, Technology and Education in Vitreous Materials, Federal University of São Carlos, 13565-905, São Carlos, SP, Brazil

ARTICLE INFO

Keywords:
Niobium
Lithium borate glasses
^{93}Nb solid-state NMR
Glass structure

ABSTRACT

The scientific and technological interest in niobium-bearing materials has significantly increased in recent years. Still, reports on the structural details about the short- and medium-range order of the intermediate oxide Nb_2O_5 in glasses are quite scarce. In this work, the structural mechanisms underlying the incorporation of niobium oxide into lithium metaborate glass spanning concentrations up to ~25 mol % are investigated through standard and advanced solid-state nuclear magnetic resonance and Raman spectroscopies. The commonly encountered NbO_6 distorted octahedral coordination occurs across the entire range of concentrations. With increasing niobia content, systematic changes in the speciation of the three-coordinated boron units are observed, revealing a progressive increase in the concentration of $BO_{3/2}$ trigonal sites at the expense of anionic $BO_{2/2}O^-$ groups. Furthermore, heteronuclear dipolar ^{7}Li–^{93}Nb, and unprecedented $^{11}B^{(III)}$–^{93}Nb and $^{11}B^{(IV)}$–^{93}Nb recoupling experiments reveal an increase in all of the dipolar interaction strengths, reflecting the formation of B-O-Nb connectivities with increasing Nb_2O_5 content.. Above 10 mol % Nb_2O_5, the Raman spectra suggest the onset of niobium-oxide clustering. Altogether, these results suggest that niobium acts as a network former in alkali borate glasses, which is in consonance with the structural role reported for Nb_2O_5 in alkali silicate and phosphate glasses.

1. Introduction

Niobium (Nb), the 41st element of the periodic table, is a 4d transition metal characterized by its small ionic radius and high cationic field strength in the pentavalent state. In the Nb^{5+} (d^0) oxidation state within an octahedral coordination environment, these ions tend to configure as out-of-center distorted polyhedra due to the second-order Jahn-Teller effect [1]. Such a distortion is recognized as a key mechanism underlying important properties of niobium-bearing materials, such as non-linear optical behavior.

In the realm of glass and glass-ceramic science, niobium oxide has been increasingly investigated as a constituent in various glass matrices [2–10]. The incorporation of niobium into optical devices such as optical fibers and fiber amplifiers is of great interest due to their high refractive indices, while maintaining transparency over a wide spectral range encompassing both the visible and infrared regions [11]. Research efforts have, therefore, focused on elucidating the impact of niobium oxide on material properties and its structural role within the glass network, often described as that of an intermediate oxide.

In general, the insertion of polyvalent oxides into alkali silicate, borate, and phosphate glass matrices offers an avenue to increase the overall mechanical, thermal, and hydrolytic stability of these materials. Specifically, borate glasses are remarkable for their low melting temperatures, wide glass-forming ranges, good glass stability against crystallization, and compatibility concerning rare-earth and transition metal incorporation [12]. Lithium borate glass matrices have promising applications and functionalities, including radiation shielding, solar energy conversion, photonics, lithography, vacuum ultraviolet optics, *etc.* [13], while their combination with Nb_2O_5 in glasses and glass-ceramics has garnered particular interest in the solid electrolyte field [14–17].

The further development of these materials requires a fundamental understanding of the effect of niobium oxide on the physical properties of borate glasses in terms of the short- to medium-range structural ordering [18]. For example, the fraction of three- and four-coordinated

* Corresponding author.
E-mail address: rbpena@ifsc.usp.br (R.B. Pena).

https://doi.org/10.1016/j.jnoncrysol.2025.123912
Received 4 September 2025; Received in revised form 24 October 2025; Accepted 2 December 2025
Available online 30 December 2025

boron is an important observable that can be related to various macroscopic glass properties, such as thermal and mechanical stability [19,20]. To this end, solid-state nuclear magnetic resonance (NMR) stands out as a powerful technique providing detailed structural insights – from bonded neighbors, coordination numbers, and site symmetries (along with their quantification), to more extended features such as connectivity, interatomic correlations, and cationic spatial distribution. These latter aspects are particularly accessible, even in multicomponent glasses, via advanced NMR pulse-sequences through selective measurement of magnetic interactions between the NMR active nuclei [21].

In pursuit of this aim, the present study investigates glasses of composition $x$$Nb_2O_5$–(100−$x$)$LiBO_2$, keeping the molar ratio $R = Li_2O/B_2O_3$ fixed at $R = 1$ at the metaborate joint, which lies outside the compositional region of liquid-liquid immiscibility [22]. To the best of our knowledge, the present contribution is the first structural study of such a ternary alkali-borate glass system using a comprehensive set of standard and advanced multinuclear solid-state NMR techniques, combined with Raman spectroscopy.

2. Experimental methods

Glass samples were prepared in final batches of 8 g using the conventional splat-quenching method. Powder mixtures of dry H_3BO_3 (Alfa Aesar, 99.8 %), Li_2CO_3 (Synth, P.A.), and Nb_2O_5 (CBMM, >99.99 %) were heated in platinum crucibles in two stages up to 1050 K, poured and re-melted three times to ensure homogenization, followed by annealing to relieve internal stress. Chemical compositions were determined by inductively coupled plasma optical emission spectroscopy (ICP-OES) using an iCAP Duo 6500 Thermo spectrometer to quantify the niobium and lithium contents. Experimental values represent the average of triplicate determinations expressed in mass percent, with standard deviations within the decimal digit. Due to the use of hydrofluoric acid during sample preparation, followed by neutralization with boric acid, direct quantification of boron was not possible. Instead, boron content was inferred from the nominal metaborate composition, assuming a fixed 1:1 molar ratio with lithium. This approach enabled comparison between experimental and nominal compositions in mol percent, with deviations within ±1 mol %. Throughout this manuscript, the incorporated niobium content (x) will be represented by the experimentally determined values, as displayed in Table 1.

Buoyancy-based density measurements were conducted using an AX204 Mettler Toledo balance, with isopropyl alcohol as the immersion fluid and a set of at least five sample pieces per batch, of which the reported value represents the mean. Differential scanning calorimetry (DSC) measurements were undertaken in a Netzsch 204 differential scanning calorimeter on bulk samples with masses ranging from 15 to 20 mg, at the standard heating rate of 10 K.min^{-1} up to 873 K. The thermograms are illustrated in Fig. S.1 of the Supporting Information. Density, molar volume (calculated from the experimental glass composition), and glass transition temperature onset values are reported in Table 2. Raman spectra were measured under ambient conditions in an HR800 Evolution micro-Raman spectrometer from Horiba, using a 488 nm laser as the excitation source. The scattered light was collected by a 50× long working-distance objective using a 600 lines per millimeter grating between 10 and 2000 cm^{-1}. The position of the silicon peak (520.7 cm^{-1}) was used for calibration. Each spectrum is an average of 7 accumulations, with integration time lasting up to 80 s, recorded at a given sample position. Spectra were collected across different spatial regions, demonstrating overall homogeneity within the limits of the typical experimental variations.

Table 1
Nominal and experimental compositions of the Nb-bearing glasses with increasing niobium content within the metaborate ratio range.

Nominal Composition / mol %	Nb / m/m %	Li / m/m %	Experimental Nb_2O_5 / mol %	Experimental Li_2O / mol %
2.5 Nb_2O_5	8.0	13.9	2.1	48.9
5.0 Nb_2O_5	14.6	11.7	4.5	47.8
7.5 Nb_2O_5	22.2	9.3	8.2	45.9
10.0 Nb_2O_5	27.8	9.7	9.7	45.2
15.0 Nb_2O_5	34.2	7.2	15.0	42.5
20.0 Nb_2O_5	38.5	5.7	20.3	39.9
25.0 Nb_2O_5	46.0	4.8	26.2	36.9

Table 2
Density (ρ), molar volume (V_m), and glass transition temperature (T_g) onset values for the Nb-bearing glasses with varying Nb_2O_5 content.

Nominal Composition / mol %	ρ / g.cm^{-3} (±0.02)	V_m / cm^3.mol^{-1} (±0.2)	T_g / K (±2)
2.5 Nb_2O_5	2.38	22.8	675
5.0 Nb_2O_5	2.48	24.0	690
7.5 Nb_2O_5	2.65	25.5	704
10.0 Nb_2O_5	2.74	25.8	711
15.0 Nb_2O_5	2.95	27.9	737
20.0 Nb_2O_5	3.08	30.4	752
25.0 Nb_2O_5	3.29	32.3	747

Solid-state ^{7}Li, ^{11}B, and ^{93}Nb NMR studies were carried out at room temperature at magnetic flux densities of 5.64 T, 9.40 T and 14.10 T, using as NMR spectrometers an Agilent DD2, a Bruker Avance Neo 400 MHz, and a Bruker Avance Neo 600 MHz, respectively. Commercial 1.3 mm, 2.5 mm, and 3.2 mm double or triple resonance magic-angle spinning (MAS) probes were used. ^{7}Li MAS NMR spectra were recorded at 14.10 T, using 2.5 mm rotors spun at a frequency of 18.0 kHz, using excitation pulses of 2.2 μs length and a recycle delay of 10 s. Chemical shifts are reported relative to a 1 M aqueous LiCl solution (δ_{iso}= 0 ppm). Spectra were fitted to Lorentzian lineshapes.

^{11}B MAS NMR spectra were acquired at two magnetic flux densities of 5.64 T and 14.10 T, using 3.2 mm and 2.5 mm rotors spun at a rate of 18.0 kHz. A recycle delay of 20 s was employed to ensure complete relaxation. Power levels (^{11}B nutation frequencies) were optimized to maximize signal intensity, while maintaining quantitative accuracy. Notably, ^{11}B is a quadrupolar nuclide (I = 3/2), with two distinct coordination numbers (three and four) known to exist in the glassy state. Three-coordinated ^{11}B nuclei, $B^{(III)}$, are exposed to a large electric field gradient, whose anisotropic interaction with the nuclear electric quadrupole moment significantly affects the ^{11}B MAS NMR lineshape as modeled through second-order perturbation theory. In contrast, the lineshape of the four-coordinated ^{11}B nuclei, $B^{(IV)}$, in oxide glasses can often be approximated by a simple Gaussian due to a relatively small electric field gradient. The large difference in nuclear electric quadrupole interaction strengths between $B^{(III)}$ and $B^{(IV)}$ species produces significant differences between the effective nutation behaviors of the corresponding ^{11}B nuclei, which has important bearings on the quantification of the boron sites. For accurate quantification, it is essential to apply flip angles <30° as measured for a liquid sample, and this condition was adhered to, using pulse lengths of 1.0 μs. ^{11}B chemical shifts are reported relative to BF_3-Et_2O solution, using crystalline BPO_4 (δ_{iso}= −3.5 ppm against liquid BF_3-OEt_2) as a secondary reference. The single-pulse ^{11}B MAS spectra obtained at 14.10 T were further treated by subtracting the boron nitride background signal measured on an empty rotor acquired under identical experimental conditions. Spectroscopic analyses of quadrupolar nuclei such as ^{11}B can further benefit from tracking the evolution of multiple quantum coherences under MAS conditions. These experiments enhance spectral resolution through the correlation between isotropic and anisotropic dimensions, thereby enabling the identification of overlapped spectral components and the determination of isotropic chemical shifts, δ_{iso}^{cs} and the nuclear electric quadrupolar product:

$$P_Q = C_Q\left(1 + \eta^2/3\right)^{1/2} \quad (1)$$

where C_Q and η are the nuclear electric quadrupolar coupling constant and the electric field gradient asymmetry parameter, respectively.

^{11}B Triple-Quantum (TQ) MAS NMR experiments were carried out at 160.4 MHz in a 2.5 mm probe operated at a spinning rate of 30.0 kHz, using the three-pulse z-filtering sequence [23,24]. The optimized pulse lengths (with hard pulses) for triple-quantum coherence creastion and reconversion were 3.9 μs and 1.3 μs, respectively, whereas the length of the (soft) detection pulse was 14 μs. The evolution time was incremented by 16.67 μs and 24 increments were recorded.

In this set of two-dimensional experiments, the parameters δ_{iso} and P_Q were obtained by comparing the centers of gravity of the projections in the isotropic (δ_1) and the anisotropic (δ_2) dimensions.

^{93}Nb MAS NMR experiments focused on the observation of the central $m = ½ \leftrightarrow m = -½$ Zeeman transition of the $I = 9/2$ nucleus. Spectra were measured at 9.40 T and 14.10 T, employing rotor-synchronized Hahn spin echoes in a 1.3 mm double-resonance probe at a MAS spin rate of 60.0 kHz. 90° and 180° pulse lengths were 0.4 μs and 0.8 μs for the 9.40 T acquisitions, and 1.1 μs and 2.2 μs for the 14.10 T acquisitions, respectively. A delay of 0.1 s was used in the full set of experiments acquired at both magnetic field strengths. Chemical shifts were referenced to $LiNbO_3$ ($\delta^{cs}_{iso} = -1004$ ppm relative to $NbCl_5$ solution in acetonitrile).

^{7}Li{^{93}Nb} and ^{11}B{^{93}Nb} dipolar recoupling experiments were performed with the Rotational-Echo Saturation-Pulse Double-Resonance (RESPDOR) sequence, wherein the ^{93}Nb spin system was saturated through a frequency-swept Wideband Uniform Rate Smooth Truncation (WURST) pulse, *i.e.*, the W-RESPDOR sequence [25]. In the present study, dipolar recoupling is accomplished by equalizing the ^{93}Nb population distribution over the Zeeman levels, as the resonance conditions for these transitions are passed through during the MAS rotor cycle. In the W-RESPDOR experiment, dipolar mixing times are systematically incremented via the number of MAS rotor periods [25]. Optimized WURST saturation pulse parameters for the ^{93}Nb spin-system were determined through numerical simulations, as reported in Ref.[3], and were replicated herein. All the double-resonance experiments were conducted at 14.10 T with a 20.0 kHz spin rate.

In such double-resonance experiments, the normalized ^{7}Li or ^{11}B signal amplitude differences are recorded between the spectra acquired without dipolar recoupling (*i.e.,* no ^{93}Nb irradiation, amplitude S_0) and those acquired in the presence of dipolar recoupling (*i.e.,* with WURST irradiation applied to the ^{93}Nb nuclei, amplitude S). Each of these signal amplitudes was determined by fitting a Lorentzian/Gaussian function to the corresponding S_0 and S signals of the observed ^{7}Li and ^{11}B$^{(IV)}$ signals, and by signal integration considering the combined lineshape contributions of two distinct ^{11}B$^{(III)}$ components fitted to the spectra, as discussed below. Subsequently, experimental ^{7}Li{^{93}Nb} and ^{11}B{^{93}Nb} dipolar recoupling curves are plotted as the normalized difference signal, *i.e.* $\frac{S-S_0}{S_0} = \frac{\Delta S}{S_0}$, in terms of the dipolar mixing time $n\tau_r$, the product of the number of rotor cycles (n) and the rotor cycle duration (τ_r). At sufficiently short mixing times, the dephasing can be modeled as [3]:

$$\frac{\Delta S}{S_0} \approx \frac{2}{3\pi^2} M_{2(X-Nb)} (n\tau_r)^2 \qquad \text{with } X = \text{Li, B} \qquad (2)$$

where higher-order terms can be neglected without loss of generality. Here $M_{2(X-Nb)}$ is the heteronuclear dipolar second moment characterizing the interaction of the observed nucleus X (either ^{7}Li or ^{11}B) and the non-observed ^{93}Nb nuclides. In multi-spin systems, van-Vleck second moments hold fundamental importance in characterizing the average mean square local field experienced by the nuclei under observation [26], due to dipole-dipole interactions with nuclei in their neighborhood.

3. Results, data analysis, and interpretation

3.1. Physical characterization

Fig. 1 illustrates the evolution of the density (ρ), molar volume (V_m), and glass transition temperature (T_g) as a function of the experimental Nb_2O_5 content, x. All the observables increase with increasing niobium concentration, as is often observed across a variety of oxide glass systems [3–5,7,8,11,27,28]. Within the lithium metaborate – Nb_2O_5 join, the density increases linearly with x, reaching up to 3.29±0.02 g.cm^{-3}.

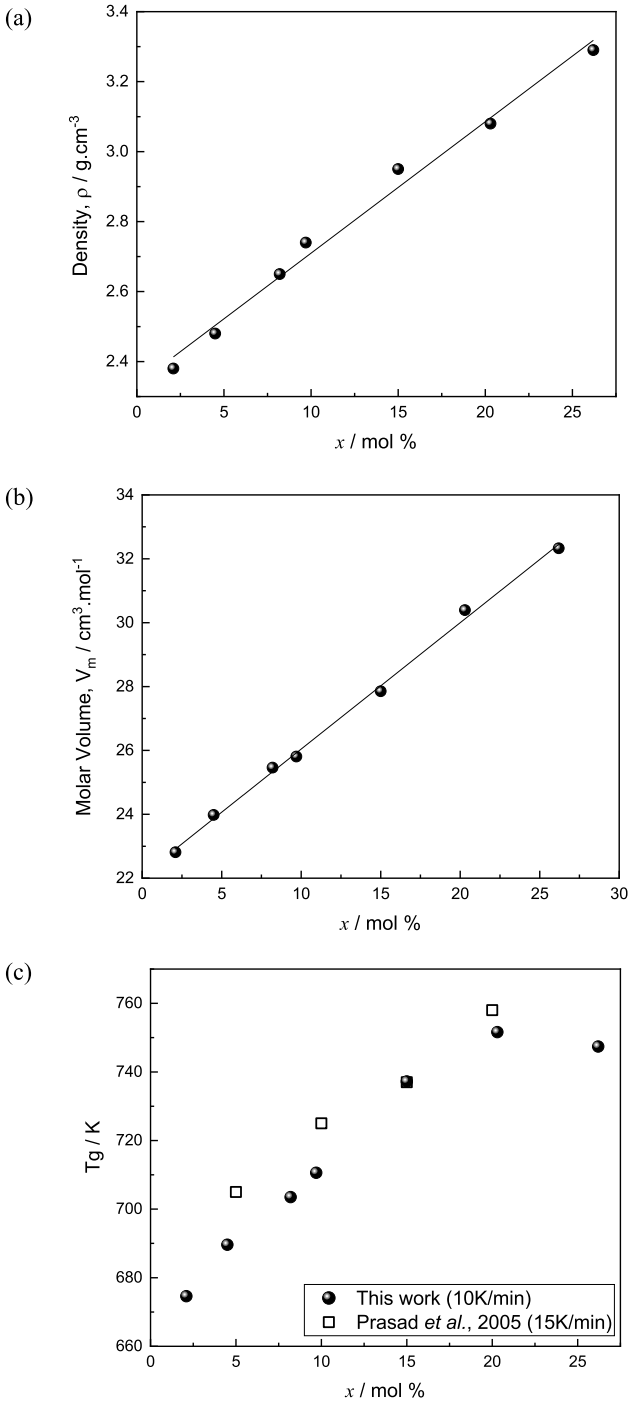

Fig. 1. (a) Density, ρ; (b) molar volume, V_m; and (c) glass transition temperature, T_g of the Nb-bearing lithium borate glasses as a function of the experimental Nb_2O_5 content, x (in mol %). The solid lines in the first two panels depict the linear regressions.

The molar volume also follows a linear trend with x, increasing by about 50 % along the series. For both properties, a linear regression of the data yields an $R^2 > 0.99$, and the corresponding empirical correlations are presented in the Supporting Information section. The glass transition temperatures (T_g) first increase and then reach a plateau value near ~750±2 K at $x = 20$ mol %, however, they were somewhat lower than those reported in Ref. 28]. For corresponding compositions, the minor discrepancy might be due to differences regarding the thermal histories of the as-prepared glass samples and those reported previously, or the different heating rates employed.

3.2. Raman spectra

Raman spectra of the samples under study are shown in Fig. 2, and provide important information about the borate glass structure, as well as the incorporation of niobium into the network. Raman spectra of borate glasses can typically be divided into four regions: (i) the low-wavenumber (<100 cm^{-1}) maximum depicts the Boson peak, which is a fingerprint of the vitreous state comprising the cooperative motion of nanosized domains; (ii) B-O-B bending and breathing modes of the ring structures are observed between 400 and 800 cm^{-1}; (iii) B-O stretching modes of tetrahedral units are observed between 800 and 1300 cm^{-1}, whereas (iv) B-O stretching modes of trigonal units occur in the ~1200–1600 cm^{-1} spectral range [29–31].

The Raman spectrum of undoped lithium metaborate glass ($x = 0$) displays an asymmetric band centered around 770 cm^{-1}, which arises from the combined contributions of the symmetric ring breathing vibrations of ring structures containing four-coordinated boron ($B^{(IV)}$) and vibrational modes due to chain type metaborates ($BO_{2/2}O^-$) [29, 32–34]. The bands located at ~950 cm^{-1} and ~1100 cm^{-1} are attributed to the characteristic B-O vibration of chain-type metaborates and diborate units, respectively [32]. Similarly, the wavenumber region between 1200 and 1600 cm^{-1} provides structural information about trigonal units with varying degrees of polymerization, which are assumed to be mostly of the $BO_{2/2}O^-$ type [34,35]. The high polarizability of Nb^{5+} and the large Raman cross-section of the associated Nb-O vibrational modes [8] result in significant changes in the vibrational spectrum relative to that of the lithium metaborate base glass even for small amounts of Nb_2O_5. Consequently, spectroscopic features reflecting the superstructural organization of borate rings, as typically observed in the intermediate wavenumber range, are obscured by the dominant contributions of the Nb-O vibrations.

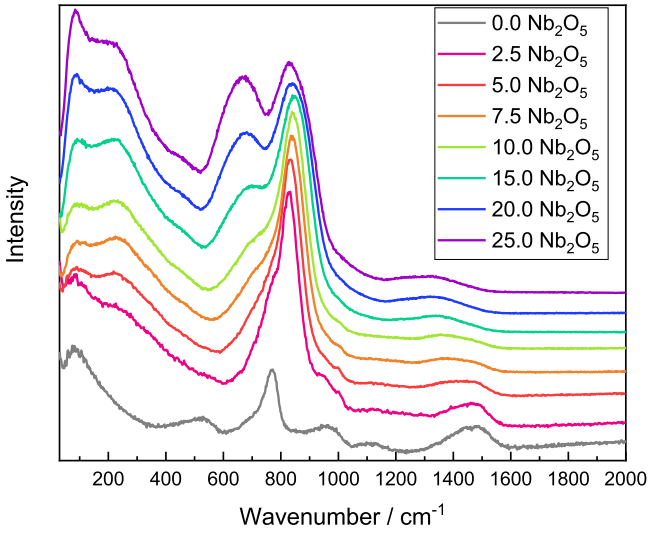

Fig. 2. Raman spectra of the Nb-bearing lithium borate glasses as a function of the nominal Nb_2O_5 content. The spectra are offset vertically to improve visual clarity.

Upon the insertion of Nb_2O_5, we observe the appearance of Raman scattering in the low (200–300 cm^{-1}) and intermediate (600–900 cm^{-1}) wavenumber regions, the latter of which can be attributed to characteristic vibrational modes of six-coordinated niobium species [36]. Based on the insights derived from Raman spectra of crystalline niobium oxide compounds, the vibrational mode located at ~230 cm^{-1} is due to the bending of the Nb-O-Nb linkages [36], and the broad band at ~650 cm^{-1} is assigned to the symmetric Nb-O stretching modes within the Nb^{VI} octahedra [36]. Notably, amorphous thin films of Nb_2O_5 and Ta_2O_5 show Raman scattering peaks near the same spectral region. Given that the atomic weight of Nb is roughly half that of Ta, one may conclude that oxygen is the principal element involved in the vibrational motion [37]. In niobium oxides, the lower characteristic wavenumbers of the stretching modes correlate with longer Nb-O bonds or higher polyhedral regularity [38]. In turn, the ~800 cm^{-1} band is attributed to the antisymmetric stretching mode of Nb-O-Nb linkages [36].

In niobium-bearing borate glasses, the vibrational band at around 650 cm^{-1} has been assigned to vibrations of terminal oxygen atoms of NbO_6 units linked to BO_3 units [10,39]. Indeed, for the glass system examined in this study, the vibrational scattering observed in the intermediate wavenumber region becomes increasingly significant for compositions with $x > 10$ mol %, consistent with the NMR results to be discussed further below (see Section 3.3.4). Finally, the signals in the high-wavenumber region (1100–1600 cm^{-1}) are assigned to various types of trigonal boron species. A significant redshift of the high-wavenumber envelope is observed in this region, which at first glance would suggest depolymerization of the borate network, in analogy to findings in other metaborate glasses containing transition and post-transition metal ions [30]. For samples with $x > 10$ mol %, a band in the range ~ 600–700 cm^{-1} emerges, and becomes increasingly prominent as x increases. This spectral feature is generally associated with niobium-oxide clustering, reflecting increasing levels of Nb-O-Nb linkages. In the related literature, such an assignment is based on the resemblance of the resulting spectrum to the vibrational modes of orthorhombic crystalline compounds, configuring local arrangements of corner-sharing $NbO_{6/2}$ octahedra [7,8].

3.3. Solid-state NMR spectra

3.3.1. ^7Li MAS NMR

Fig. 3 shows the ^7Li MAS NMR spectra, as well as the evolution of the ^7Li isotropic chemical shift and full width at half maximum (*FWHM*) as a function of the Nb_2O_5 content, which are also summarized in Table 3. Owing to the small electric quadrupole moment of the ^7Li nuclide, the quadrupolar coupling strength is generally weak, allowing for a reasonable description of the central $m = ½ \leftrightarrow m = -½$ transition using symmetric functions, within the limit of first-order perturbation theory. Lorentzian, rather than Gaussian functions, were used to simulate the ^7Li MAS NMR spectra, effectively reproducing the experimental lineshape. The latter may indicate a high lithium ionic mobility at ambient temperature, but this is not confirmed by static ^7Li NMR measurements (see Fig. S.2 in the Supporting Information section), which essentially exhibit Gaussian lineshapes with linewidths exceeding 5.9 kHz, as typically found for the ^7Li NMR linehapes in the slow-motion regime. As evidenced by Fig. 3b, there is a subtle low frequency shift of δ_{iso} – beyond the experimental uncertainty – accompanied by a decrease in linewidths as the Nb_2O_5 content increases. Such behavior could stem from increased shielding of the ^7Li nuclei by the surrounding electronic environment, possibly due to the increasing extent of Li-Nb interactions. This issue will be further investigated using advanced double resonance NMR protocols, as detailed in Section 3.3.4.

3.3.2. ^{11}B MAS NMR

Fig. 4 illustrates the ^{11}B MAS NMR spectra as a function of niobium content recorded at 5.64 T and 14.10 T, along with the curve-fit. As displayed in Table 4, an estimation of the $B^{(IV)}$ fraction, N_4, can be

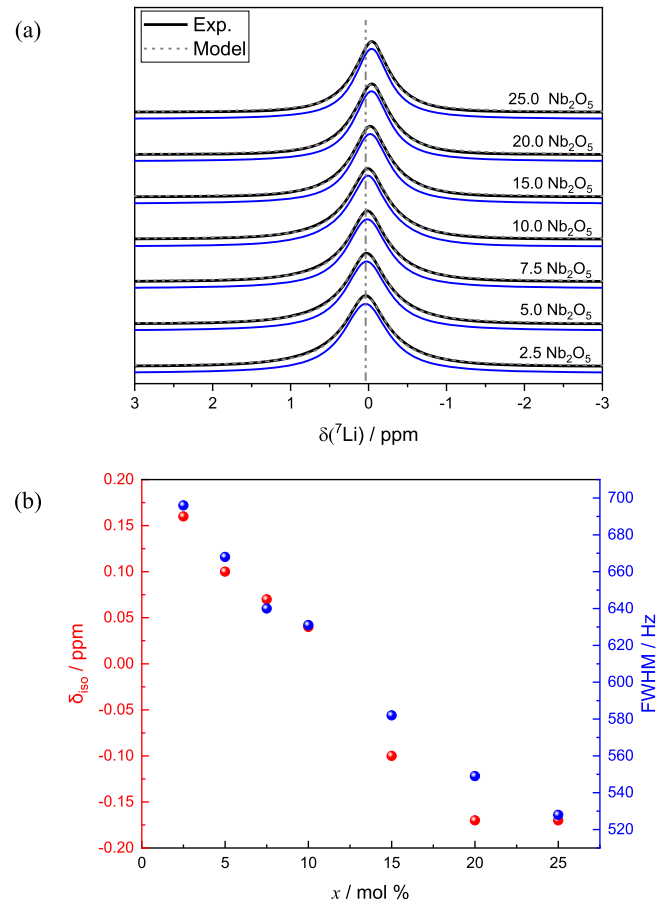

Fig. 3. (a) ^{7}Li MAS NMR spectra (black curves) along with their lineshape fits (blue curves) using a single Lorentzian function and (b) the evolution of the isotropic chemical shift and linewidth as a function of the experimental Nb_2O_5 content, *x*. The dashed line marks the chemical shift of the 2.5 mol % Nb_2O_5 glass as a guide for the eyes.

Table 3
^{7}Li MAS curve fit parameters for the Nb-bearing glasses with varying Nb_2O_5 content.

Nominal Composition / mol %	δ_{iso} / ppm (±0.05)	*FWHM* / Hz (± 5)
2.5 Nb_2O_5	0.16	696
5.0 Nb_2O_5	0.10	668
7.5 Nb_2O_5	0.07	640
10.0 Nb_2O_5	0.04	631
15.0 Nb_2O_5	−0.10	582
20.0 Nb_2O_5	−0.17	549
25.0 Nb_2O_5	−0.17	528

determined from the integral of the corresponding ^{11}B MAS spectra acquired at higher magnetic field strength, where the $B^{(III)}$ and $B^{(IV)}$ lineshape components exhibit little to no overlap. Due to the multiple parameters required for the curve fit, measuring at two different magnetic flux densities provides additional physical constraints for an appropriate spectral decomposition. The set of data measured at both magnetic field strengths was simulated by considering one Gaussian component for $B^{(IV)}$ and – across the entire composition range – two distinct quadrupolar components for $B^{(III)}$, corresponding to symmetric and asymmetric units, $B_S^{(III)}$ and $B_A^{(III)}$, as detailed in the following. Because of the strong directional covalent bonding in three-coordinate boron oxides, the $^{11}B_{S,A}^{(III)}$ quadrupole coupling parameters are confined within rather narrow, well-defined regions (*e.g.* see Ref. [40,41]), and these are used as constraints in the iterative fitting process according to the mean values reported for glassy $LiBO_2$ therein [42]. The $B^{(IV)}$ species are generally assumed to be linked to bridging O atoms only and are, in the following, denoted $BO_{4/2}^-$ units. $B_S^{(III)}$ groups are assumed to be connected to three bridging O atoms $(BO_{3/2})$, while $B_A^{(III)}$ units are linked to two bridging and one non-bridging O atoms, $BO_{2/2}O^-$ units.

To further validate the curve fitting model, ^{11}B TQMAS NMR experiments were carried out for selected glass compositions: 0, 2.5, 15.0, and 25.0 Nb_2O_5. The bidimensional spectra, displayed in Fig. S.3 of the Supporting Information section, exhibit two distinct regions of cross-peaks corresponding to $B^{(III)}$ and $B^{(IV)}$ moieties. Despite the improved resolution offered by the second dimension, a pronounced overlap remains for the $B^{(III)}$ components, indicating that these species possess similar quadrupolar and chemical shift distributions. Average isotropic chemical shifts (δ_{iso}) and second-order quadrupolar shifts (P_Q) were extracted by determining the center of gravity of the $B^{(III)}$ and $B^{(IV)}$ signal regions [23]. The resulting values, summarized in Table S.1 (see Supporting Information), are in excellent agreement with those presented in Table 4, thereby confirming the reliability of the ^{11}B MAS NMR parameters upon niobium incorporation. A detailed view of the $B^{(III)}$ region for the 2.5 and 25 Nb_2O_5 glasses is displayed in Fig. 5. For the 2.5 Nb_2O_5 glass, the $^{11}B^{(III)}$ TQMAS trace along the δ_2 dimension (extracted for $\delta_1 =$ 21.8 ppm) is shown on the right panel of Fig. 5a. Disregarding the distortions in the powder pattern caused by the triple-quantum excitation during the ^{11}B TQMAS experiment, a reasonable simulation of the trace-spectrum could be obtained, which represents the main features of the quadrupolar powder-pattern. The simulation parameters are: $\delta_{iso}=$ 18.8 ± 0.5 ppm, $C_Q = 2.58 \pm 0.05$ MHz and $\eta_Q = 0.40 \pm 0.05$, where the uncertainties were estimated considering variations in the parameters which still result in visually acceptable agreement with the ^{11}B MAS spectra. For the 25 mol % Nb_2O_5 glass, the ^{11}B TQMAS spectrum reveals the presence of two partially resolved ^{11}B signals (Fig. 5b, right panel). Two horizontal traces extracted from the 2D spectrum at $\delta_1 = 19.6$ ppm and 22.0 ppm – chosen to minimize mutual overlap – allowed an independent evaluation of the local parameters. The δ_{iso} and P_Q values derived from the (δ_1, δ_2) centers of gravity of both signals were 17.3 ppm and 18.1 ppm, and 2.6 MHz and 2.8 MHz, respectively. Unfortunately, due to the extensive spectral overlap between both $B^{(III)}$ components, reliable quadrupolar asymmetry parameter (η) values could not be determined from simulations of the TQMAS traces for this sample. Taken together, ^{11}B TQMAS results corroborate the parameters obtained from the simulations of the ^{11}B MAS at the two different magnetic field strengths (Table 4), thereby confirming their reliability and the structural quantitative analysis, as follows.

For the lithium metaborate base glass, NMR investigations probing ^{11}B and ^{10}B nuclides indicate that approximately 40 % of the boron nuclei are four-coordinated, $B^{(IV)}$ units [42,43]. Assuming these species to be mono-anionic $BO_{4/2}^-$ units, the charge balance at a unitary lithium-to-boron ratio would also require the $B^{(III)}$ units to be either mono-anionic $BO_{2/2}O^-$, *i.e.* metaborate species, which is consistent with the Raman spectrum (Section 3.2), or a superposition of neutral, mono-anionic, and di-anionic trigonal species. Regarding their local symmetry and interaction with the magnetic field, mono-anionic trigonal planar units display a non-axial local symmetry of the electric field gradient (EFG) tensor due to the presence of one non-bridging oxygen, resulting in asymmetry parameters of $0.4 \leq \eta_Q \leq 0.6$. In a similar vein, a di-anionic pyroborate unit, $BO_{1/2}(O^-)_2$ is predicted to have an asymmetry parameter significantly different from zero, whereas a fully polymerized neutral three-coordinated boron $(BO_{3/2})$ would exhibit nearly cylindrical local symmetry, with relatively low values of the EFG asymmetry parameter ($\eta_Q \leq 0.2$). At the $LiBO_2$ composition, the anionic asymmetric $B^{(III)}$ units have been estimated in the literature to account for 54 % of the total NMR signal, whereas <10 % of the total ^{11}B MAS NMR signal is assigned to the neutral $(BO_{3/2})$ units [42].

The ^{11}B MAS NMR spectra of the ternary glasses can be analyzed analogously, as detailed in Table 4. For glasses with $x < 10$ mol %

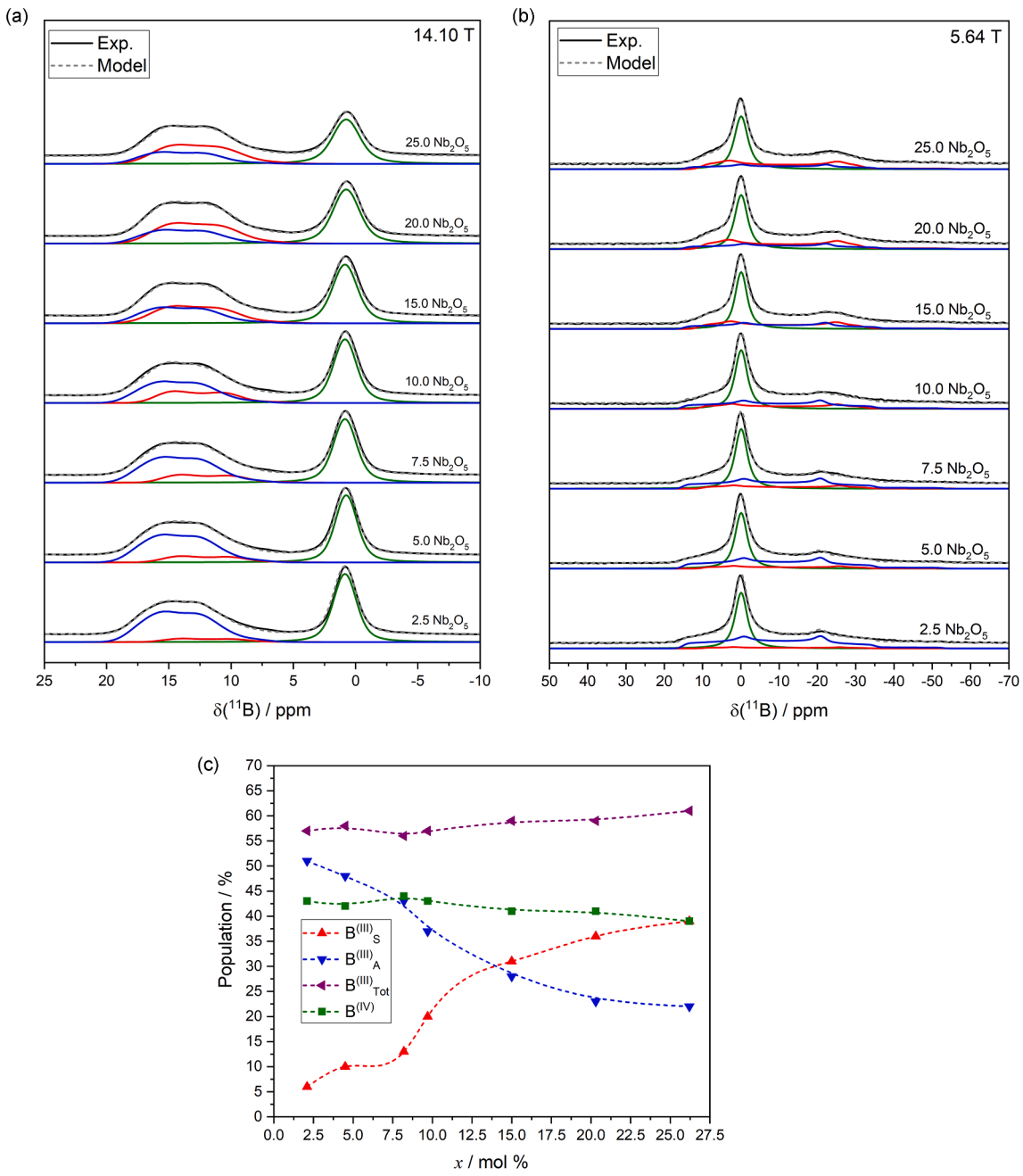

Fig. 4. Curve-fit of the ^{11}B MAS NMR spectra recorded at (a) 14.10 T and (b) 5.64 T; and (c) estimated $B_S^{(III)}$ $B_A^{(III)}$ $B_{Tot}^{(III)}$ and $B^{(IV)}$ fractions as a function of the experimental Nb_2O_5 content, x. The dashed curves in the latter are guides for the eyes.

Nb_2O_5, the spectroscopic parameters resemble closely those of lithium metaborate glass, and the fraction of $B^{(IV)}$ species and the spectroscopic parameters remain approximately constant, while the relative proportions between the two different $B^{(III)}$ components account for a major part of the spectral distinctions. For glasses with $x > 10$ mol %, the ^{11}B MAS NMR lineshapes of the three-coordinated boron species are distinctly different, which can be properly fit by also changing the quadrupolar parameters of the $B^{(III)}$ species. A detailed view of these components at the lower flux density, where the quadrupolar effect is more evident on the lineshapes, is displayed in Fig. S.4 in the Supporting Information section. As indicated by Fig. 4c, N_4 remains constant up to a Nb_2O_5 content of ~10 mol % and decreases slightly for higher niobium concentrations. For an approximately constant fraction of the three-coordinated boron species, the major effect of niobium oxide incorporation is a systematic increase of the fraction of symmetric $B_S^{(III)}$ ($BO_{3/2}$) units along with a decrease of the fraction of asymmetric $B_A^{(III)}$ ($BO_{2/2}O^-$) units. This compositional trend is consistent with a network former role of niobium oxide, as it diminishes the overall degree of anionic modification of the network former boron oxide: the contribution of the fully polymerized trigonal $(BO_{3/2})$ units increases continuously from low concentrations in glassy $LiBO_2$ to significant levels (*ca.* 30 - 40 %) with increasing Nb_2O_5 content. This systematic change is reflected by a continuous decrease in the combined concentrations of the anionic $BO_{4/2}^-$ and $BO_{2/2}O^-$ groups. This implies that the Nb_2O_5 component is present as an anionic species, which attracts part of the Li_2O.

3.3.3. *^{93}Nb MAS NMR*

^{93}Nb MAS NMR spectra were acquired at two different magnetic flux densities, using a rotor-synchronized Hahn-spin echoes to avoid signal

Table 4
^{11}B MAS curve fit parameters for the Nb-bearing glasses with varying Nb_2O_5 content. Estimated experimental errors are ±0.1 ppm and ±0.5 ppm for $\delta_{iso}(B^{(IV)})$ and $\delta_{iso}(B^{(III)})$, respectively, and ±0.05 MHz for $C_Q(B^{(III)})$.

Nominal Composition / mol. %	B_0 / T	$B^{(IV)}$ Integration p / % ±1	$B^{(III)}$ δ_{iso} ppm	C_Q / MHz	η_Q ±0.05	p/% ±1	$B^{(IV)}$ δ_{iso} / ppm	*FWHM* / ppm	p/% ±1
2.5 Nb_2O_5	5.64		16.6			6	0.0	1.54	42
	14.10	42	18.8			52			
						6	0.9	1.54	43
						51			
5.0 Nb_2O_5	5.64	–	16.7			10	0.0	1.54	42
	14.10	42	18.8			48			
				2.65	0.20	10	0.8	1.54	42
						48			
7.5 Nb_2O_5	5.64	–	16.7	2.60	0.40	13	0.0	1.59	43
	14.10	42	18.8			44			
						13	0.8	1.59	44
						43			
10.0 Nb_2O_5	5.64	–	17.3			20	0.0	1.64	43
	14.10	42	18.9			37			
						20	0.8	1.64	43
						37			
15.0 Nb_2O_5	5.64	–	17.5		0.20	32	0.0	1.71	40
	14.10	42	18.8		0.38	28			
						31	0.8	1.71	41
						28			
20.0 Nb_2O_5	5.64	–	17.5	2.65	0.18	36	0.0	1.81	40
	14.10	41	18.6	2.64	0.38	24			
						36	0.7	1.81	41
						23			
25.0 Nb_2O_5	5.64	–				36	0.7	1.81	43
					0.18	21			
	14.10	39	17.4			39	0.0	1.81	39
			18.4		0.35	22			

distortions caused by coil-ringing [3]. The MAS NMR spectra are affected by the combined effect of chemical shift anisotropy and a wide distribution of nuclear electric quadrupole coupling strengths [44], which result in a somewhat asymmetric central signal, accompanied by a pattern of several spinning sidebands. The asymmetric profile of the dominant central MAS NMR peak, with a lineshape tailing towards low frequency is typical of many central Zeeman transition spectra of quadrupolar nuclei in glasses. Such lineshapes can be understood and simulated based on second-order perturbation theory, assuming a wide distribution of electric field gradients. As intrinsic to the glassy state, the structural disorder is accounted for by considering a normal statistical distribution for the components of the EFG tensor. The *Czjzek* model describes the quadrupolar interaction by the probability $P(C_Q,\eta)$ of finding local environments with values of the quadrupole coupling constant C_Q and the asymmetry parameter η_Q, such that [45,46]:

$$P(C_Q,\eta) = \frac{C_Q^4 \eta_Q}{\sqrt{2\pi}\sigma^5}\left(1-\frac{{\eta_Q}^2}{9}\right)\exp\left[-\frac{C_Q^2}{2\sigma^2}\left(1+\frac{{\eta_Q}^2}{3}\right)\right] \quad (3)$$

Here, σ is the width of the distribution or the standard deviation of the elements of the EFG tensor. Notably, the application of the Czjzek model implies a fixed η_Q value of 0.62. In the case of ^{93}Nb NMR in glasses, a significant complication in analyzing the spectra arises from the presence of a considerable chemical shift anisotropy (*CSA*), producing sets of spinning sidebands flanking the central MAS NMR peak. Simulations capturing these effects using the MRSimulator python library [47] enabled the determination of the average parameters δ_{iso}, $|\overline{C_Q}|$, and *CSA* from the spectra, as displayed in Table 5. The magnetic shielding and the electric field gradient tensors are assumed to be coincident, along the lines of simplified analyses used previously for Nb_2O_5-$NaPO_3$ [5].

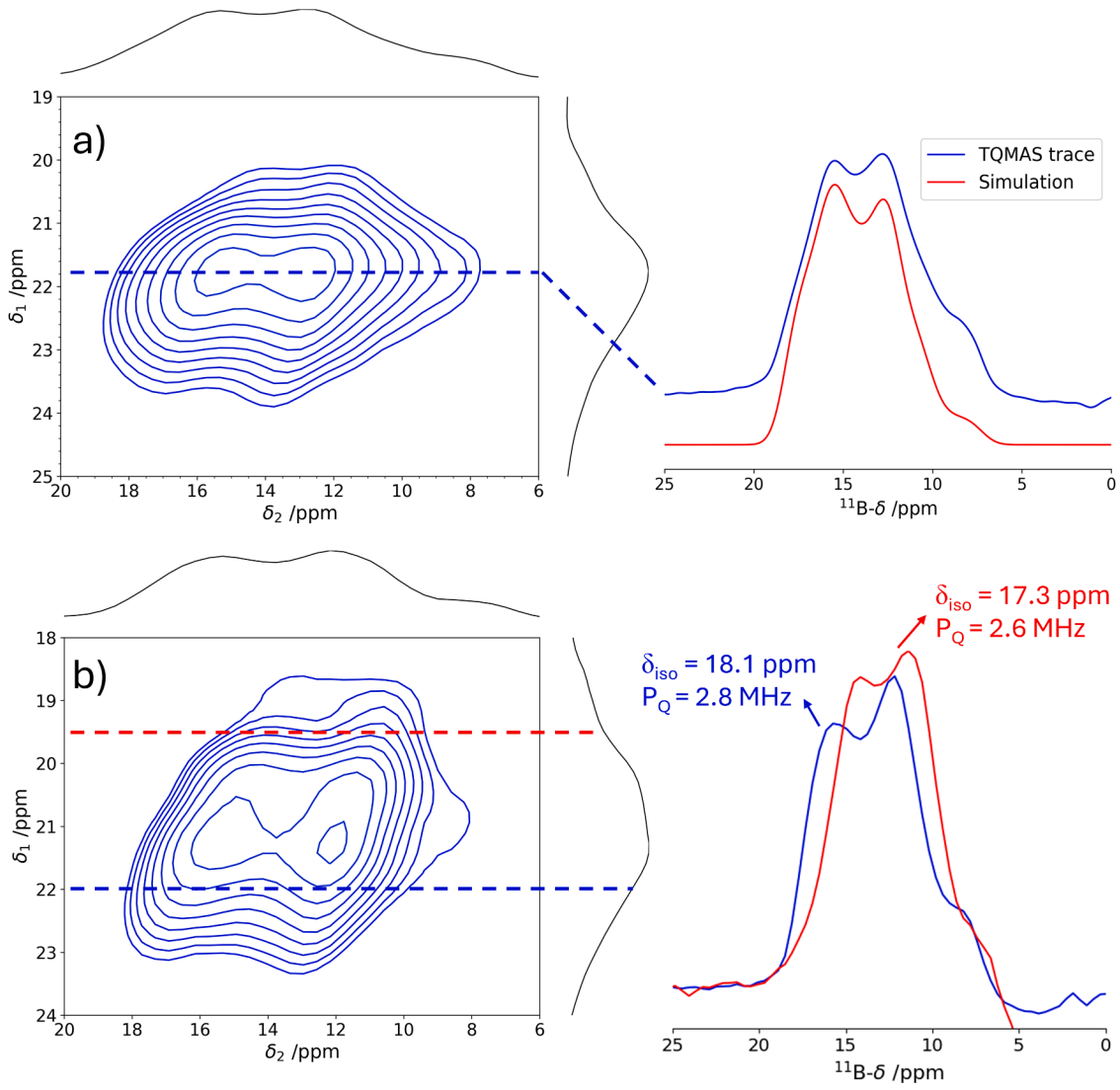

Fig. 5. (a) Detailed view of the $B^{(III)}$ region of the ^{11}B TQMAS NMR spectrum for the 2.5 and 25 Nb_2O_5 glasses (parts a and b respectively). In (a) the horizontal trace extracted for $\delta_1 = 21.8$ ppm is shown, along with a simulation of the ^{11}B second-order quadrupolar powder pattern under MAS condition, with δ_{iso}= 18.8 ppm, C_Q = 2.58 MHz and $\eta = 0.40$. In (b) horizontal traces extracted at $\delta_1 = 19.6$ and 22.0 ppm are shown. The derived isotropic chemical shift (δ_{iso}) and quadrupolar coupling constant (P_Q) values for each component are displayed in the plot.

Table 5
Isotropic chemical shifts δ_{iso}, average of the magnitude of the quadrupole coupling constant, $|\overline{C_Q}|$ and chemical shift anisotropy, $\delta_{aniso}=\delta_{33}-\delta_{iso}$ retrieved from curve-fit ^{93}Nb MAS NMR acquired at two distinct magnetic flux densities, and heteronuclear second moments $M_{2(X-Nb)}$ with X = Li or B determined from the parabolic fits to Eq.(2) of the experimental W-RESPDOR curves for the Nb-bearing glasses with varying Nb_2O_5 content.

Nominal Composition / mol %	δ_{iso} / ppm (±10)	$\lvert\overline{C_Q}\rvert$ / MHz (±0.7)	δ_{aniso} / ppm (±10)	$M_{2(Li-Nb)}$ / 10^6 rad^{2}s^{-2} (±20 %)	$M_{2(BIV-Nb)}$ / 10^6 rad^{2}s^{-2} (±20 %)
2.5 Nb_2O_5	−1007	28.0	−470	3	4
5.0 Nb_2O_5	−1019	29.4	−400	11	6
7.5 Nb_2O_5	−1029	29.4	−370	19	7
10.0 Nb_2O_5	−1039	30.0	−310	21	5
15.0 Nb_2O_5	−1057	28.4	−310	32	33
20.0 Nb_2O_5	−1068	29.0	−370	39	31
25.0 Nb_2O_5	−1071	28.4	−370	45	51

Although the superposition of multiple Nb species cannot be ruled out, the ensemble of spectra could still be effectively fitted using a single Czjzek distribution across the entire composition range analyzed for both magnetic field strengths, namely 9.40 T and 14.1 T, as shown in Fig. 6, with the parameters summarized in Table 5.

By comparing the ^{93}Nb δ_{iso} values spanning the –1070 to –1010 ± 10 ppm range, with the ^{93}Nb chemical shift scale established for crystalline model compounds [44,48], we conclude that the niobium species are six-coordinated within the entire glass-forming range, as also commonly encountered in other glass systems. As depicted in Fig. 6c, the systematic trend of δ_{iso} towards more negative values with increasing Nb_2O_5 content signifies progressive changes to the local niobium environment with composition, showing a more pronounced variation up to 15 mol % Nb_2O_5, and a more subtle change at higher x-values (see Supporting Information for details). Interestingly, the addition of Nb_2O_5 into lithium-silicate and -borate glass systems leads to opposite trends: in silicates the δ_{iso} value tends to increase (displaying less negative values) with increasing Nb contents [3,4], whereas in the $NaPO_3$-Nb_2O_5 system, the presence of multiple niobium sites makes a straightforward comparison in this regard impossible [5]. In turn, the correlation between the ^{93}Nb isotropic chemical shift and the ionic bonding character has

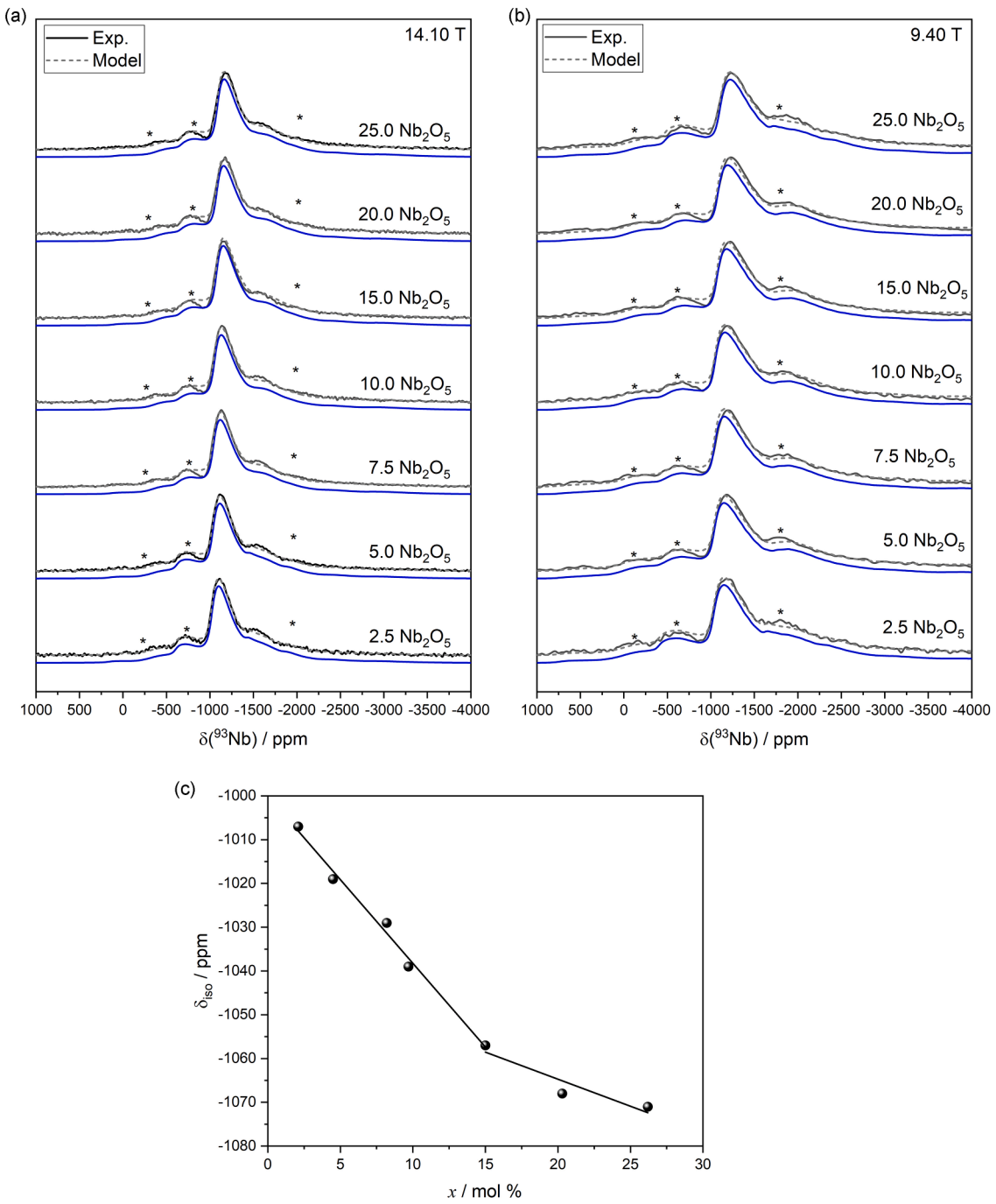

Fig. 6. ^{93}Nb central-transition MAS NMR spectra along with their curve fit using a single Czjzek function recorded at (a) 14.10 T and (b) 9.40 T and their corresponding lineshape fits with the parameters summarized in Table 5. Asterisks indicate spinning sidebands. (c) The evolution of the isotropic ^{93}Nb chemical shift as a function of the experimental Nb_2O_5 content, *x*. The solid lines show two linear regressions of the δ_{iso} trend.

been suggested, although ultra-high field ^{93}Nb MAS NMR investigation on crystalline niobium-bearing compounds has indicated that corner- and edge-sharing Nb^{VI} environments cannot be straightforwardly parametrized in this fashion [44]. In terms of the average modulus $|\overline{C_Q}|$ of the ^{93}Nb quadrupole coupling constant, we find values lower than those observed in lithium silicate glasses [3], but higher than those in the sodium phosphate glasses [5]. Therefore, the distorted niobium octahedra in the glasses studied here seem to exhibit an intermediate degree of distortion compared to the phosphate and silicate reference glasses, although a detailed picture of the average local environments could benefit from further input from MD simulations.

3.3.4. *^{7}Li{^{93}Nb} and ^{11}B{^{93}Nb} W-RESPDOR*

The W-RESPDOR pulse sequence was originally conceived for measurements involving spin-1/2 observe nuclei and spin >1/2 non-observe nuclei featuring a high quadrupolar interaction strength [25,49,50], although it has also been successfully applied to observe nuclei with quadrupolar character – such as ^{11}B [51], and ^{7}Li in glass systems [3,4].

Fig. 7a compares the experimental ^{7}Li{^{93}Nb} W-RESPDOR data for the glasses with those measured for orthorhombic $LiNbO_3$. The data indicates the expected increase of dipolar interaction strength with increasing Nb/Li ratio, which is consistent with the evolution of the dipolar second moments, estimated from the parabolic fitting to Eq. (2).

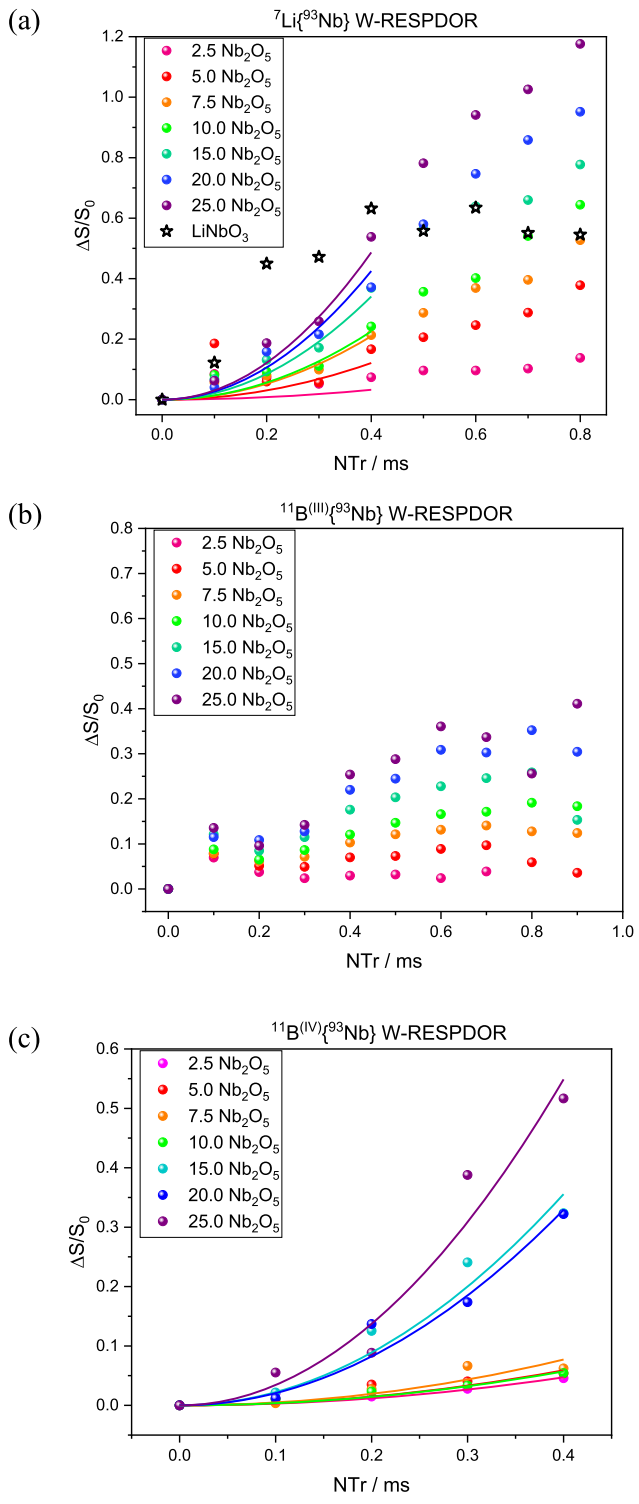

Fig. 7. W-RESPDOR experimental curves for the (a) ^{7}Li{^{93}Nb}; (b) $^{11}B^{(III)}${^{93}Nb}; (c) $^{11}B^{(IV)}${^{93}Nb} for the Nb-bearing glasses with varying Nb_2O_5 content (in mol %). Solid curves represent parabolic fits to Eq. (2).

The $M_{2(Li\text{-}Nb)}$ value measured for $LiNbO_3$ is comparable to the value expected from applying the van Vleck equation to the distance distribution present in the model compound [4]. Figs. 7b and c depict the results obtained from ^{11}B{^{93}Nb} W-RESPDOR, respectively, optimized for the $B^{(III)}$ and $B^{(IV)}$ configurations, respectively. We must advise caution, however, that the precision of the $^{11}B^{(IV)}${^{93}Nb} W-RESPDOR data is limited as these data suffer from a low signal-to-noise ratio, owing to the fast signal decay at longer mixing times due to short ^{11}B spin-spin relaxation times for these species. The evolution of the $\frac{\Delta S}{S_0}$ dephasing trends suggests that the $^{11}B^{(IV)}$-^{93}Nb dipole-dipole interaction is very weak at low niobium contents and becomes more significant above 10 mol %, where the $B^{(IV)}$ content decreases slightly, as indicated by the ^{11}B MAS NMR results. On the other hand, the $B^{(III)}$ curves show a more gradual increase in the dephasing with increasing Nb_2O_5 content. At higher niobium concentrations, given the comparable dephasing trends that indicate the formation of B-O-Nb connectivities – rather similar for both boron network former units – there is no clear evidence for preferential association of ^{93}Nb, with either $B^{(IV)}$ or $B^{(III)}$ over the other. In the latter case, separate contributions for the $BO_{2/2}O^-$ and $BO_{3/2}$ units could not be obtained from the data, and the curves extracted from their combined contributions to the W-RESPDOR curves could not be well approximated via Eq. (2). Thus, the data are of a more qualitative nature, and no second moments are extracted from them. A summary of dipolar second moments, $M_{2(X-Nb)}$, with X = Li or $B^{(IV)}$ estimated through W-RESPDOR experiments, is displayed in Table 5.

Altogether, these results are consistent with a network former role of the niobium oxide species, where the formation of six-coordinate $NbO_{6/2}^{-}$ units requires charge compensation by cationic Li^+, which tends to diminish the anionic modification of the borate network component. As a result of this conversion mechanism, the average anionic charge per borate network unit is reduced from one (in $LiBO_2$) to less than one in the Nb_2O_5-bearing glasses.

4. Discussion

When incorporated into glasses, transition metal ions can act either as network modifiers or conditional network formers, *i.e.,* as intermediate cations playing a dual structural role. From a historical approach, the designation of the network-former cation was first proposed in the seminal work of Zachariasen [52], where glass formation was attributed to covalent oxides able to form corner-sharing polyhedra. Typically, the classical network-forming species are cations with low coordination numbers – such as those configuring three or four oxygen atoms. However, octahedral coordination also satisfies the stated Zachariasen's criteria, even though octahedral units have a tendency towards forming periodic crystalline arrangements through edge- and face-sharing. Over the years, less geometrically oriented classifications were proposed, such as Sun's requirement for glass network formation based on the existence of strongly bound continuous networks [53]. In the same sense, Rawson's criterion is based on the relative stability of the metal-oxygen bonds during thermodynamic phase transitions such as melting and crystallization [54].

The effects of modifier cations in oxide glasses involve balancing the negative charge of the anionic network, while depolymerizing the glass structure by disrupting the network cross-linking through the formation of non-bridging oxygen (NBOs). In borate glasses, on the other hand, the latter structural mechanism is concurrent with changes in the boron coordination number, where three- and four-coordinated boron are canonical network formers that coexist. Over intermediate-range distances, these building blocks interconnect, forming dominantly $B^{(III)}$–O–$B^{(IV)}$ and $B^{(III)}$–O–$B^{(III)}$ linkages. Despite a situation of electrostatic repulsion, $B^{(IV)}$–O–$B^{(IV)}$ linkages are not strictly forbidden, if the concentration of charge-compensating cations is sufficiently high [55]. In the present glass system, $B^{(IV)}$–O–$B^{(IV)}$ linkages are less likely from a statistical viewpoint, as the concentrations of $B^{(IV)}$ units are rather low throughout the entire compositional region.

By including niobium into the structural framework, our data consistently indicates an octahedral coordination of niobium, combined with the progressive formation of $BO_{3/2}$ at the expense of $BO_{2/2}O^-$ units along the entire series. Equivalently, maintaining approximately the same proportion between the $B^{(III)}$ and $B^{(IV)}$ moieties, octahedrally coordinated niobium incorporates into the borate network increasing the proportion of bridging oxygen (BO) and leading to a concomitant

reduction of the NBOs. Thus, in the niobium-bearing lithium metaborate system, the network former building elements comprise three- and four-coordinate borate units, alongside six-coordinate niobium units across the composition range investigated. The data support a progressive reorganization of the network, likely with lithium cations charge-balancing $NbO_{6/2}^{-}$ units, which are formally mono-anionic. Across the Nb_2O_5-$LiBO_2$ join, niobium incorporation can be described in terms of the following melt reaction schemes involving the niobium and boron species:

$$BO_{2/2}O^{-} + NbO_{5/2} \rightarrow BO_{3/2} + NbO_{6/2}^{-} \quad (4)$$

$$BO_{4/2}^{-} + NbO_{5/2} \rightarrow BO_{3/2} + NbO_{6/2}^{-} \quad (5)$$

Both processes, as outlined in Eqs. 4 and (5), involve a partial transfer of the negative charge away from the borate towards niobium network units, therefore, implying a network former role of the niobium species. To maintain overall charge neutrality of the glass, the charge balance constraint equilibrating positive (N^{+}) and negative (N^{-}) net charges requires:

$$N^{+} = N^{-} \rightarrow N_{Li}^{+} = N_{B}^{-} + N_{Nb}^{-} \quad (6)$$

where $N_X^{\pm}$ are the charges associated with X = Li, B or Nb. Note that the average net values are retrieved by accounting for the respective N_X. For example, N_B^{-}, the total negative charge associated with the boron-based units, is calculated from the anionic boron partitioning species, disregarding the neutral $BO_{3/2}$ species, such that:

$$N_B^{-} = N_B\left[p\left(BO_{2/2}O^{-}\right) + p\left(BO_{4/2}^{-}\right)\right] \quad (7)$$

where the respective percentages p for the anionic boron species across the glass series are provided in Table 4. Based on the analytical compositions listed in Table 1, and assuming that $N_{Li} = N_B$ within the $LiBO_2$-Nb_2O_5 join, the quantitative partition of each term in the charge balance process is summarized in Table 6. To test the robustness of this approach, analogous calculations conducted based on the nominal contents produced similar results. Aside from the glass sample with the lowest Nb_2O_5 content, where large deviations are observed between both values — possibly arising from the 20 % discrepancy of the nominal and the experimental Nb content — the discrepancies are otherwise within the uncertainties for the ensemble of glass compositions investigated herein. The calculations further indicate that, following the incorporation mechanisms described by Eqs. (4) and (5), the charge transfer is complete up to x = 15 mol %, signifying that the average charge on the six-coordinate Nb species is unity. Towards higher Nb contents (about 20 and 25 mol %), the charge transfer per niobium species appears to decrease, suggesting that a fraction of the niobium species is uncharged, which may indicate the onset of niobium-oxide clustering. This could imply, beyond the network former effect into the borate-based primary network, the formation of a secondary niobium-based network. This structural scenario is consistent with the overall spectroscopic picture furnished by combining the strong increase in Raman scattering in the range ~ 600–700 cm^{-1} (Fig. 2), and the composition dependence of the ^{93}Nb isotropic chemical shift (Fig. 5). These spectroscopic changes most likely signify the appearance of Nb-O-Nb linkages, which are commonly taken as an indication of the clustering in the glass network [5,20]. The occurrence of edge-sharing cannot be ruled out, although it is neither straightforwardly evidenced nor excluded by our spectroscopic data.

Dipolar recoupling measurements, conducted through ^{7}Li{^{93}Nb} and ^{11}B{^{93}Nb} W-RESPDOR experiments, indicate increasing Li-O-Nb and $B^{(III)}$-O-Nb and $B^{(IV)}$-O-Nb interactions in this composition range, whereas $B^{(IV)}$-O-Nb interactions are largely absent at low Nb_2O_5 contents. Previous double-resonance NMR studies on binary alkali borate glasses with alkali content up to 30 mol % report a statistical distribution of the modifier cations within the glass structure, without appreciable preference for their association with either $B^{(III)}$ or $B^{(IV)}$ units [56–58]. Likewise, no structural bias toward $B^{(III)}$-O-Nb or $B^{(IV)}$-O-Nb configurations has been observed at the higher niobium compositions.

Recent results obtained by Extended X-ray Absorption Fine Structure (EXAFS) analysis of the Nb K-edge in other Nb-bearing materials indicate characteristic spectral features associated with corner-sharing octahedra in lanthanum borate glasses [10]. Besides, X-ray Absorption Near Edge Structure (XANES) investigation of the $L_{2,3}$-edges of niobium in a set of minerals has revealed a mixed covalent character in the Nb-O bonding [59]. Within the scope of NMR techniques, ^{17}O NMR investigations are of paramount importance [60], despite the requirement for dedicated ^{17}O labelling during sample preparation. As an extension of the stated definitions, experimental evidence indicating a corner-sharing configuration, a more covalent bonding nature, and/or the direct formation of BOs would further support the conclusion that niobium assumes a network former role in lithium metaborate glasses. Finally the increased average coordination number associated with the incorporation of increasing amounts of six-coordinate Nb into the glass structure, as well as with the increase in the fraction of $BO_{3/2}$ at the expense of the $BO_{2/2}O^{-}$ units may account for the increase in the glass transition temperature with increasing x, as shown in Fig. 1c.

In varying glass compositions, systematic investigations of Nb-bearing borate glasses comprising Li_2O to B_2O_3 molar ratios (R) below unity are valuable to comprehensively understand the behavior of niobium in borates, as well as the complete or partial substitution of lithium in ternary, quaternary or more complex glass systems. Interestingly, the full replacement of lithium with sodium through the conventional splat-quenching preparation method spans only a narrow glass formation range [61], suggesting significant structural differences between both glass systems. In a broader perspective, the structural study conducted herein will aid in the comprehension of analogous d^0 transition metal elements in glasses, where intrinsic polyhedral distortions are at play. In terms of advanced solid-state NMR techniques, this contribution reveals fertile ground for extending the W-RESPDOR pulse sequence protocols to examine glasses configuring both observed and non-observed heteronuclei with strong quadrupolar interactions.

Table 6
Quantitative partition of total positive net charge from lithium (N_{Li}^{+}), total negative net charge from boron (N_B^{-}), and average negative net charge from niobium (N_{Nb}^{-}/N_{Nb}) in the niobium-bearing lithium metaborate glasses, based on the analytical compositions listed in Table 1. Values in parentheses include analogous calculations based on the nominal contents.

Nominal Composition / mol %	N_{Li}^{+}	N_B^{-}	N_{Nb}	N_{Nb}^{-}/N_{Nb}
2.5 Nb_2O_5	97.8	91.9	4.2	1.4(1.0)±0.4
5.0 Nb_2O_5	95.6	86.0	9.9	1.1(1.0)±0.2
7.5 Nb_2O_5	91.8	79.4	16.4	0.8(0.7)±0.2
10.0 Nb_2O_5	90.4	72.3	19.4	0.9(0.9)±0.1
15.0 Nb_2O_5	85.0	58.2	30.0	0.9(0.9)±0.1
20.0 Nb_2O_5	79.8	51.0	40.3	0.7(0.7)±0.1
25.0 Nb_2O_5	73.8	46.1	52.4	0.5(0.6)±0.1

5. Conclusions

Herein, ternary niobium lithium metaborate glasses with compositions $x$$Nb_2O_5$–(100−$x$)$LiBO_2$ were prepared up to the threshold level of niobium incorporation (x ~ 25 mol %), and were structurally characterized by combining solid-state NMR and Raman spectroscopies. Niobium incorporates into the network as distorted anionic NbO_6 octahedra acting as a network-forming unit throughout the entire glass series, reducing the overall anionic charge on the borate species via an incorporation mechanism described by Eqs. (4) and (5). For niobium concentration ranging from 10 to 15 mol %, pronounced structural modifications are evidenced by a change in the ^{93}Nb chemical shift trend, combined with a subtle decrease in N_4 values and a systematic

change in the concentrations of $BO_{2/2}O^-$ and $BO_{3/2}$ moieties. Raman spectra suggest the formation of Nb-O-Nb clusters at niobium oxide contents exceeding 10 mol %. Double-resonance NMR techniques reveal that even at low niobium concentrations, lithium cations indeed serve as charge compensators for anionic $NbO^-_{6/2}$ units. At Nb_2O_5 contents below 10 mol %, the niobium species associate preferentially with the $B^{(III)}$ species, while at higher concentrations, niobium associates with $B^{(III)}$ and $B^{(IV)}$ moieties without evidence of preferential interaction with one over the other. In turn, the W-RESPDOR pulse sequence demonstrates strong potential for state-of-the-art investigations of nuclides previously deemed challenging for NMR studies of glassy materials.

Data availability

The data supporting the findings of this study are available from the corresponding author, RBP, upon reasonable request.

CRediT authorship contribution statement

Rafaella Bartz Pena: Writing – original draft, Visualization, Methodology, Investigation, Formal analysis, Data curation, Conceptualization. **Henrik Bradtmüller:** Writing – review & editing, Methodology, Investigation, Conceptualization. **Laureano Ensuncho:** Writing – review & editing, Investigation. **Marcos De Oliveira:** Writing – review & editing, Investigation. **Hellmut Eckert:** Writing – original draft, Supervision, Resources, Project administration, Methodology, Funding acquisition, Conceptualization.

Declaration of competing interest

The authors declare that they have no known competing financial interests or personal relationships that could have appeared to influence the work reported in this paper.

Acknowledgements

The authors gratefully acknowledge Prof. Dr. Edgar D. Zanotto and Prof. Dr. Paulo S. Pizani for granting access to the LaMaV and GEOR laboratory facilities at the Federal University of São Carlos. We are very thankful to José Rodrigues da Silva (LaMaV, UFSCar) for his invaluable assistance in producing the glass samples, and Dr. Rafael Bonacin de Oliveira (LaMaV, UFSCar) for the support in the buoyancy-based density measurements and thoughtful discussions on niobium-bearing glasses. The experimental characterizations were carried out using equipments from the Center for Research, Technology and Education in Vitreous Materials (CeRTEV), funded by São Paulo Research Foundation (FAPESP), under the process number 2013/07793–6. The use of the 9.4 T spectrometer was possible thanks to FAPESP process 2019/12885–3 (multiuser equipment). The authors are thankful to FAPESP for funding this research through the post-doctoral and doctoral fellowship grants n° 2023/17069–5 (RBP), 2019/26399–3 (HB), and 2022/01937–5 (LE). HE, MOJr and HB acknowledge the Brazilian National Council for Scientific and Technological Development (CNPq) for research grants under n° 310870/2020–8, 312802/2023–4 and 309285/2025–9, respectively. This work was partially presented at the 17th PNCS International Conference in Tsukuba: "*NMR Perspectives on Niobium-Bearing Glasses: A Case Study on the Lithium Metaborate Composition*".

References

[1] M. Kunz, I.D. Brown, Out-of-center distortions around octahedrally coordinated d^0 Transition metals, J. Solid. State Chem. 115 (1995) 395–406.
[2] M.R. Cicconi, K. Kimura, H. Bradtmüller, H. Deng, S. Kohara, Y. Onodera, T. Hayakawa, S. Shimono, K. Hayashi, D. de Ligny, Unraveling the structural complexity of niobate units in aluminosilicate glasses and glass–ceramics, Mater. Adv. 6 (2025) 3863–3874.
[3] H. Bradtmüller, Q. Zheng, A. Gaddam, H. Eckert, E.D. Zanotto, Structural impact of niobium oxide on lithium silicate glasses: results from advanced interaction-selective solid-state nuclear magnetic resonance and Raman spectroscopy, Acta Mater. 255 (2023) 119061.
[4] W. Zielasko, R.B. Oliveira, E.D. Zanotto, M.R. Hansen, H. Eckert, H. Bradtmüller, Contrasting structural roles of Nb_2O_5 *vs.* La_2O_3 in silicate glasses: a quantitative solid-state NMR study, Acta Mater. 297 (2025) 121343.
[5] L. Ensuncho, H. Bradtmüller, P.S. Salmon, H. Eckert, Structural role of Nb_2O_5 in phosphate glasses: an advanced solid-state NMR protocol for the glass system xNb_2O_5 – (100-x)$NaPO_3$, J. Am. Chem. Soc. 147 (34) (2025) 31147–31164, 2025.
[6] J.H. Faleiro, N.O. Dantas, A.C.A. Silva, H.P. Barbosa, B.H.S.T. da Silva, K.d. O. Lima, G.d.F. Silva, R.R. Gonçalves, R. Falci, Y. Messadeq, I.D.O. Branco, B. M. Cerrutti, H. Bradtmüller, H. Eckert, J.L. Ferrari, Niobium incorporation into rare-earth doped aluminophosphate glasses: structural characterization, optical properties, and luminescence, J. Non -Cryst. Solids 605 (2023) 122173.
[7] M.R. Cicconi, D.K. Dobesh, B. Schroeder, T. Otsuka, T. Hayakawa, D. de Ligny, Alkali-niobate aluminosilicate glasses: structure and properties, Opt. Mater.: X 18 (2023) 100228.
[8] T. Komatsu, T. Honma, T. Tasheva, V. Dimitrov, Structural role of Nb_2O_5 in glass-forming ability, electronic polarizability and nanocrystallization in glasses: a review, J. Non. Cryst. Solids. 581 (2022) 121414.
[9] L.M. Marcondes, H. Bradtmüller, S.N. Carvalho dos Santos, L.K. Nolasco, C. R. Mendonça, S.H. Santagneli, G.Y. Poirier, M. Nalin, Structural and luminescence characterization of europium-doped niobium germanate glasses and glass-ceramics: novel insights from ^{93}Nb solid-state NMR spectroscopy, Ceram. Int. 48 (2022) 20801–20808.
[10] R.O. Alekseev, L.A. Avakyan, G.Y. Shakhgildyan, G.A. Komandin, V.I. Savinkov, N. A. Romanov, A.A. Veligzhanin, S.P. Lebedev, A.M. Ermakova, G.B. Sukharina, Local atomic structure of the high refractive index La_2O_3–Nb_2O_5–B_2O_3 glasses, J. Alloys. Compd. 917 (2022) 165357.
[11] S. Sanghi, S. Rani, A. Agarwal, V. Bhatnagar, Influence of Nb_2O_5 on the structure, optical and electrical properties of alkaline borate glasses, Mater. Chem. Phys. 120 (2010) 381–386.
[12] M. Bengisu, Borate glasses for scientific and industrial applications: a review, J. Mater. Sci. 51 (2016) 2199–2242.
[13] V. Dua, S.K. Arya, K. Singh, Review on transition metals containing lithium borate glasses properties, applications and perspectives, J. Mater. Sci. 58 (2023) 8678–8699.
[14] P.-N. Huang, X.-H. Huang, The influence of MO_2, M_2O_5 and MO_3 oxides on the conductivity of lithium borate glasses, Solid State Ion. 36 (1989) 59–63.
[15] K. Singh, P.R. Gandhi, B.M. Chaudhari, Use of ferroelectric materials to modify cationic conduction of the Li_2O: B_2O_3 amorphous solid electrolyte system, Solid State Ion. 28 (1988) 752–755.
[16] M.P.F. Graça, M.G.F. da Silva, M.A. Valente, Influence of thermal and thermoelectric treatments on structure and electric properties of B_2O_3–Li_2O–Nb_2O_5 glasses, J. Non. Cryst. Solids. 354 (2008) 901–908.
[17] M.P.F. Graça, M.G.F. da Silva, M.A. Valente, $NaNbO_3$ crystals dispersed in a B_2O_3 glass matrix–Structural characteristics *versus* electrical and dielectrical properties, Solid State Sci. 11 (2009) 570–577.
[18] A.C. Wright, G. Dalba, F. Rocca, N.M. Vedishcheva, Borate *versus* silicate glasses: why are they so different? Phys. Chem. Glas-Eur. J. Glass Sci. Technol. B 51 (2010) 233–265.
[19] M.S. Bødker, J.C. Mauro, R.E. Youngman, M.M. Smedskjaer, Statistical mechanical modeling of borate glass structure and topology: prediction of superstructural units and glass transition temperature, J. Phys. Chem. B 123 (2019) 1206–1213.
[20] X. Lu, L. Deng, J. Du, J.D. Vienna, Predicting boron coordination in multicomponent borate and borosilicate glasses using analytical models and machine learning, J. Non. Cryst. Solids. 553 (2021) 120490.
[21] H. Eckert, Spying with spins on messy materials: 60 years of glass structure elucidation by NMR spectroscopy, Int. J. Appl. Glass. Sci. 9 (2018) 167–187.
[22] R.R. Shaw, D.R. Uhlmann, Subliquidus immiscibility in binary alkali borates, J. Am. Ceram. Soc. 51 (1968) 377–382.
[23] A. Medek, J.S. Harwood, L. Frydman, Multiple-quantum magic- angle spinning NMR: a new method for the study of quadrupolar nuclei in solids, J. Am. Chem. Soc. 117 (1995) 12779–12787.
[24] J.P. Amoureux, F.C. Fernandez, S. Steuernagel, Z filtering in MQMAS NMR, J. Magn. Reson. 123 (1996) 116–118.
[25] A.-L. Wübker, J. Koppe, H. Bradtmüller, L. Keweloh, D. Pleschka, W. Uhl, M. R. Hansen, H. Eckert, Solid-state nuclear magnetic resonance techniques for the structural characterization of geminal alane-phosphane frustrated Lewis pairs and secondary adducts, Chem. Eur. J. 27 (2021) 13249–13257.
[26] H. Eckert, S. Elbers, J.D. Epping, M. Janssen, M. Kalwei, W. Strojek, U. Voigt, Dipolar solid state NMR approaches towards medium-range structure in oxide glasses, Topics in Current Chemistry 246 (2004) 195–233.
[27] B.V.R. Chowdari, Z. Rong, Studies on the role R_2O_n (R= Ga and Cr, n= 3; R= Nb and Ta, n= 5) in 0.5 Li_2O 0.5{xR_2O_n·(1− x) B_2O_3} glass system, Mater. Sci. Eng.: B 53 (1998) 241–255.
[28] N.S. Prasad, K.B.R. Varma, Evolution of ferroelectric $LiNbO_3$ phase in a reactive glass matrix ($LiBO_2$–Nb_2O_5), J. Non. Cryst. Solids. 351 (2005) 1455–1465.
[29] E.I. Kamitsos, G.D. Chryssikos, Borate glass structure by Raman and infrared spectroscopies, J. Mol. Struct. 247 (1991) 1–16.
[30] D. Möncke, E.I. Kamitsos, D. Palles, R. Limbach, A. Winterstein-Beckmann, T. Honma, Z. Yao, T. Rouxel, L. Wondraczek, Transition and post-transition metal ions in borate glasses: borate ligand speciation, cluster formation, and their effect on glass transition and mechanical properties, J. Chem. Phys. 145 (2016) 124501.

[31] E.O. Gomes, J. Andrés, F. Tielens, G. Lelong, D. de Ligny, B. Moulton, Unravelling the structural origin of vibrations in crystalline lithium triborate, LiB_3O_5, 2024.. 10.2139/ssrn4832819.
[32] W.L. Konijnendijk, J.M. Stevels, The structure of borate glasses studied by Raman scattering, J. Non. Cryst. Solids. 18 (1975) 307–331.
[33] L. Song, Y. Wang, A.C. Hannon, S.A. Feller, W. Li, Y. Zhou, F. Zhu, Structural investigation of lithium borate glasses by Raman spectroscopy: quantitative evaluation of structural units and its correlation with density, J. Non. Cryst. Solids. 616 (2023) 122478.
[34] T. Yano, N. Kunimine, S. Shibata, M. Yamane, Structural investigation of sodium borate glasses and melts by Raman spectroscopy.: I. Quantitative evaluation of structural units, J. Non. Cryst. Solids. 321 (2003) 137–146.
[35] J.A. Kapoutsis, E.I. Kamitsos, G.D. Chryssikos, H.A. Feller, N. Lower, M. Affatigato, S.A. Feller, Synthesis and vibrational investigation of lithium magnesium metaborate glasses, Phys. Chem. Glas 41 (2000) 321–324.
[36] J.M. Jehng, I.E. Wachs, Structural chemistry and Raman spectra of niobium oxides, Chem. Mater. 3 (1991) 100–107.
[37] F.L. Galeener, W. Stutius, G.T. McKinley, Electron microscopy and Raman spectroscopy of Nb_2O_5, Ta_2O_5 and Si_3N_4 thin films. The Physics of MOS Insulators, Elsevier, 1980, pp. 77–81.
[38] F.D. Hardcastle, I.E. Wachs, Determination of niobium-oxygen bond distances and bond orders by Raman spectroscopy, Solid State Ion. 45 (1991) 201–213.
[39] W.D. Fragoso, C. de Mello Donegá, R.L. Longo, A structural model of La_2O_3–Nb_2O_5–B_2O_3 glasses based upon infrared and luminescence spectroscopy and quantum chemical calculations, J. Non. Cryst. Solids. 351 (2005) 3121–3126.
[40] S. Kroeker, J.F. Stebbins, Three-coordinated boron-11 chemical shifts in borates, Inorg. Chem. 40 (2001) 6239–6246.
[41] P.M. Aguiar, S. Kroeker, Boron speciation and non-bridging oxygens in high-alkali borate glasses, J. Non. Cryst. Solids. 353 (2007) 1834–1839.
[42] Y.H. Yun, P.J. Bray, B^{11} nuclear magnetic resonance studies of Li_2O-B_2O_3 glasses of high Li_2O content, J. Non. Cryst. Solids. 44 (1981) 227–237.
[43] S.A. Feller, W.J. Dell, P.J. Bray, ^{10}B NMR studies of lithium borate glasses, J. Non. Cryst. Solids. 51 (1982) 21–30.
[44] O.B. Lapina, D.F. Khabibulin, K.V. Romanenko, Z. Gan, M.G. Zuev, V. N. Krasil'nikov, V.E. Fedorov, ^{93}Nb NMR chemical shift scale for niobia systems, Solid State Nucl. Magn. Reson. 28 (2005) 204–224.
[45] J.-B.d.E. de Lacaillerie, C. Fretigny, D. Massiot, MAS NMR spectra of quadrupolar nuclei in disordered solids: the Czjzek model, J. Magn. Reson. 192 (2008) 244–251.
[46] G. Czjzek, J. Fink, F. Götz, H. Schmidt, J.M.D. Coey, J.P. Rebouillat, A. Liénard, Atomic coordination and the distribution of electric field gradients in amorphous solids, Phys. Rev. B 23 (1981) 2513.
[47] D.J. Srivastava, M. Giammar, M.C. Venetos, L. McCarthy-Carney, P.J. Grandinetti, MRSimulator: a cross-platform, object-oriented software package for rapid solid-state NMR spectral simulation and analysis, J. Chem. Phys. 161 (2024) 212501.
[48] O.B. Lapina, D.F. Khabibulin, A.A. Shubin, V.V. Terskikh, Practical aspects of ^{51}V and ^{93}Nb solid-state NMR spectroscopy and applications to oxide materials, Prog. Nucl. Magn. Reson. Spectrosc. 53 (2008) 128–191.
[49] Z. Gan, Measuring multiple carbon–nitrogen distances in natural abundant solids using R-RESPDOR NMR, Chem. Commun. 45 (2006) 4712–4714.
[50] E. Nimerovsky, R. Gupta, J. Yehl, M. Li, T. Polenova, A. Goldbourt, Phase-modulated LA-REDOR: a robust, accurate and efficient solid-state NMR technique for distance measurements between a spin-1/2 and a quadrupole spin, J. Magn. Reson. 244 (2014) 107–113.
[51] R.W. Dorn, A.L. Paterson, I. Hung, P.L. Gor'kov, A.J. Thompson, A.D. Sadow, Z. Gan, A.J. Rossini, Dipolar heteronuclear correlation solid-state NMR experiments between half-integer quadrupolar nuclei: the case of ^{11}B–^{17}O, J. Phys. Chem. C 126 (2022) 11652–11666.
[52] W.H. Zachariasen, The atomic arrangement in glass, J. Am. Chem. Soc. 54 (1932) 3841–3851.
[53] K.-H. Sun, Fundamental condition of glass formation, J. Am. Ceram. Soc. 30 (1947) 277–281.
[54] E.A. Chechetkina, Rawson's criterion and intermolecular interactions in glass-forming melts, J. Non. Cryst. Solids. 128 (1991) 30–47.
[55] P. Lv, B. Stevensson, Y. Yu, T. Wang, M. Edén, BO_3/BO_4 intermixing in borosilicate glass networks probed by double-quantum ^{11}B NMR: what factors govern BO_4–BO_4 formation? J. Phys. Chem. C 127 (2023) 20026–20040.
[56] E. Ratai, J.C.C. Chan, H. Eckert, Local coordination and spatial distribution of cations in mixed-alkali borate glasses, Phys. Chem. Chem. Phys. 4 (2002) 3198–3208.
[57] S.P. Puls, H. Eckert, Spatial distribution of lithium ions in glasses studied by ^{7}Li {^{6}Li} spin echo double resonance, Phys. Chem. Chem. Phys. 9 (2007) 3992–3998.
[58] J.D. Epping, W. Strojek, H. Eckert, Cation environments and spatial distribution in Na_2O–B_2O_3 glasses: new results from solid state NMR, Phys. Chem. Chem. Phys. 7 (2005) 2384–2389.
[59] Q. Bollaert, M. Chassé, H. Elnaggar, A. Juhin, A. Courtin, L. Galoisy, C. Quantin, M. Retegan, D. Vantelon, G. Calas, Niobium speciation in minerals revealed by $L_{2,3}$-edges XANES spectroscopy, Am. Mineral. 108 (2023) 595–605.
[60] J.F. Stebbins, P. Zhao, S. Kroeker, Non-bridging oxygens in borate glasses: characterization by ^{11}B and ^{17}O MAS and 3QMAS NMR, Solid State Nucl. Magn. Reson. 16 (2000) 9–19.
[61] D. Burnett, D. Clinton, R.P. Miller, Some phase relationships within the system $Na_2O/B_2O_3/Nb_2O_5$, J. Mater. Sci. 3 (1968) 47–60.